Available online at www.sciencedirect.com
SCIENCE DIRECT®
Journal of Sound and Vibration 262 (2003) 187–197
JOURNAL OF SOUND AND VIBRATION
www.elsevier.com/locate/jsvi

Letter to the Editor

A parameter estimation method for the flexural wave properties of a beam

Andrew J. Hull*, David A. Hurdis

Submarine Sonar Department, Naval Undersea Warfare Center Division, Newport, RI 02841, USA

Received 25 February 2002; accepted 2 September 2002

1. Introduction

Measuring the flexural wave properties of beams is important because these parameters significantly contribute to the static and dynamic response of structures. An effective approach for obtaining such measurements relies on an "inverse" method that typically involves choosing a model of the system under study and fitting experimental data to the model by letting the unknown parameters be free variables.

One of the first researchers to examine what is called the inverse problem was Prony [1], who developed a technique for estimating the parameters of damped sinusoids from evenly spaced measurements. Today, the "Prony methods," which describe the majority of equally spaced multisensor experimental techniques, are most notably used by Grosh and Williams [2], who have developed a modified version that deconvolves the helical wave spectrum of a point-driven cylindrical shell using simulated data. Their procedure first estimates the wavenumbers using a root-finding algorithm applied to a characteristic polynomial and then relies on the resulting values to find the response coefficients with a least-squares algorithm.

Another proponent of the inverse method was Ram [3], whose technique when applied to a flexural beam uses eigenvalue and eigenvector data to build a model of a discretized system from which mass and stiffness parameters can be extracted. In addition, Linjama and Lahti [4], Bauman [5], and Mace and Halkyard [6] have estimated structural intensity and its corresponding properties (usually shear force, transverse velocity, bending moment, and angular velocity) in a beam. There is also an inverse technique described by Koss and Karczub [7] that uses the response coefficients to estimate the strain field in a beam; however, it does not solve explicitly for the flexural wavenumber. In still another study, McDaniel et al. [8] show how transient loading provides a means to estimate frequency-dependent damping, as well as investigate the transfer of data from the spatial domain into the wavenumber domain. Finally, McDaniel and Shepard [9]

*Corresponding author.
E-mail address: hullaj@npt.nuwc.navy.mil (A.J. Hull).

0022-460X/03/$ - see front matter
doi:10.1016/S0022-460X(02)01384-6

have proposed a solution to the inverse problem that is based on the use of unevenly spaced measurements and an iterative method for determining the flexural wavenumber.

In the work presented in this paper, an inverse method is developed to measure the complex flexural wavenumber and the corresponding response coefficients of a beam that is undergoing transverse motion. Transforming experimental measurements into parameter estimates, in this case, will result in a closed-form solution. The technique is typically used for measuring the flexural wave properties of cars, ships, aircraft, bridges, buildings, and other common structures that contain beams.

More specifically, the inverse technique described here combines seven transfer function measurements to yield closed-form values of flexural wavenumber and response coefficients at any given test frequency. Numerical simulations are presented to show the results of the method when noise is added to simulated data. An experiment is also conducted on a beam, during which the method is applied to the measurement data to yield the flexural wavenumber and the response coefficients of an actual system. When the estimated transfer function is calculated from these estimated parameters and compared to the original measured data, it is found that the parameter estimation method is extremely accurate.

It should be noted that the inverse process can easily incorporate beam parameter perturbations, making it an ideal method for design alteration testing. If the material properties of the beam change, the method can be simply rerun with the newly designed beam and the original experimental setup. Because the process is independent of boundary conditions, it is not necessary to duplicate the beam-mounting conditions, which is especially useful when the rotational and translational compliance of the mount may change from experiment to experiment. Furthermore, the inverse method is independent of beam length, allowing comparisons between beams of varying length. Finally, the calculations needed to compute flexural wavenumber parameters can be done in seconds, which permits real-time evaluations of beam properties.

2. System model and inverse solution

The system model of the transverse motion of the beam is the Bernoulli–Euler beam equation, written as

$$EI\frac{\partial^4 u(x,t)}{\partial x^4}+\rho A_b\frac{\partial^2 u(x,t)}{\partial t^2}=0, \tag{1}$$

where x is the distance along the length of the beam (m), t is the time (s), u is the displacement of the beam in the (transverse) y direction (m), E is the (complex) Young's modulus (N/m^2), I is the moment of inertia (m^4), ρ is the density (kg/m^3), and A_b is the cross-sectional area of the beam (m^2). Implicit in Eq. (1) is the assumption that plane sections remain plane during bending (or transverse motion). Additionally, Young's modulus, the moment of inertia, the density, and the cross-sectional area remain constant along the entire length of the beam. The displacement is modelled as a steady state response in time and is expressed as

$$u(x,t)=U(x,\omega)\exp(\mathrm{i}\omega t), \tag{2}$$

where ω is the frequency of excitation (rad/s), $U(x,\omega)$ is the temporal Fourier transform of the transverse displacement, and $\mathrm{i} = \sqrt{-1}$. The temporal solution to Eq. (1), derived using Eq. (2) and written in terms of trigonometric functions, is

$$U(x,\omega) = A(\omega)\cos[\alpha(\omega)x] + B(\omega)\sin[\alpha(\omega)x] + C(\omega)\cosh[\alpha(\omega)x] + D(\omega)\sinh[\alpha(\omega)x], \tag{3}$$

where $A(\omega)$, $B(\omega)$, $C(\omega)$, and $D(\omega)$ are response coefficients and $\alpha(\omega)$ is the flexural wavenumber given by

$$\alpha(\omega) = \left[\frac{\omega^2}{(EI/\rho A_b)}\right]^{1/4}. \tag{4}$$

For brevity, the ω dependence is omitted from the response coefficients and the flexural wavenumber throughout the remainder of the paper. Note also that Eqs. (3) and (4) are independent of boundary conditions and that the inverse model developed here does not require boundary condition specifications or assumptions.

Eq. (3) has five unknowns and is non-linear with respect to the unknown flexural wavenumber. It will be shown that the use of seven independent, equally spaced measurements allows the five unknowns to be estimated with closed-form solutions. To begin, all the seven frequency-domain transfer functions of acceleration (or displacement) are measured at some location and are then divided by a common reference measurement. Each of the seven transfer functions is collected by two accelerometers placed at different locations on the beam (although one may be placed at the base of the shaker table). The seven measurements are set equal to the theoretical expression given in Eq. (3). Without loss of generality, the middle measurement location corresponds to $x = 0$—a location that does not necessarily have to be placed at the middle of the beam. The seven equations are written as

$$T_{-3} = \frac{U_{-3}(-3\delta,\omega)}{V_0(\omega)} = A\cos(3\alpha\delta) - B\sin(3\alpha\delta) + C\cosh(3\alpha\delta) - D\sinh(3\alpha\delta), \tag{5}$$

$$T_{-2} = \frac{U_{-2}(-2\delta,\omega)}{V_0(\omega)} = A\cos(2\alpha\delta) - B\sin(2\alpha\delta) + C\cosh(2\alpha\delta) - D\sinh(2\alpha\delta), \tag{6}$$

$$T_{-1} = \frac{U_{-1}(-\delta,\omega)}{V_0(\omega)} = A\cos(\alpha\delta) - B\sin(\alpha\delta) + C\cosh(\alpha\delta) - D\sinh(\alpha\delta), \tag{7}$$

$$T_0 = \frac{U_0(0,\omega)}{V_0(\omega)} = A + C, \tag{8}$$

$$T_1 = \frac{U_1(\delta,\omega)}{V_0(\omega)} = A\cos(\alpha\delta) + B\sin(\alpha\delta) + C\cosh(\alpha\delta) + D\sinh(\alpha\delta), \tag{9}$$

$$T_2 = \frac{U_2(2\delta,\omega)}{V_0(\omega)} = A\cos(2\alpha\delta) + B\sin(2\alpha\delta) + C\cosh(2\alpha\delta) + D\sinh(2\alpha\delta) \tag{10}$$

and

$$T_3 = \frac{U_3(3\delta,\omega)}{V_0(\omega)} = A\cos(3\alpha\delta) + B\sin(3\alpha\delta) + C\cosh(3\alpha\delta) + D\sinh(3\alpha\delta), \tag{11}$$

where δ is the sensor-to-sensor separation distance (m) and $V_0(\omega)$ is the reference measurement. Note that the transfer functions given in Eqs. (5)–(11) are dimensionless.

Eq. (7) is added to Eq. (9) and Eq. (6) is added to Eq. (10), yielding

$$A\cos(\alpha\delta) + C\cosh(\alpha\delta) = \frac{T_1 + T_{-1}}{2} \tag{12}$$

and

$$A\cos(2\alpha\delta) + C\cosh(2\alpha\delta) = \frac{T_2 + T_{-2}}{2}. \tag{13}$$

Eqs. (8), (12) and (13) are combined and manipulated using multiple-angle regular and hyperbolic trigonometric expressions to produce

$$\cosh(\alpha\delta)\cos(\alpha\delta) - \left\{\left(\frac{T_1 + T_{-1}}{2T_0}\right)[\cosh(\alpha\delta) + \cos(\alpha\delta)]\right\} + \left(\frac{T_2 + T_{-2} + 2T_0}{4T_0}\right) = 0. \tag{14}$$

It is noted at this point that a zero-finding algorithm applied to Eq. (14) is sufficient to solve for the unknown flexural wavenumber and the corresponding response coefficients. This process produces an estimation of five parameters using five measurements. However, a closed-form solution of the flexural wavenumber is preferred because zero-finding algorithms are sometimes unstable and occasionally yield a solution that corresponds to the wrong zero, which would require further mathematical manipulation. Thus, Eq. (7) is subtracted from Eq. (9), Eq. (6) is subtracted from Eq. (10) and Eq. (5) is subtracted from Eq. (11), resulting in

$$B\sin(\alpha\delta) + D\sinh(\alpha\delta) = \frac{T_1 - T_{-1}}{2}, \tag{15}$$

$$B\sin(2\alpha\delta) + D\sinh(2\alpha\delta) = \frac{T_2 - T_{-2}}{2} \tag{16}$$

and

$$B\sin(3\alpha\delta) + D\sinh(3\alpha\delta) = \frac{T_3 - T_{-3}}{2}, \tag{17}$$

respectively. Eqs. (15)–(17) are combined and manipulated using multiple-angle regular and hyperbolic trigonometric expressions to give

$$\cosh(\alpha\delta)\cos(\alpha\delta) - \left\{\left[\frac{T_2 - T_{-2}}{2(T_1 - T_{-1})}\right][\cosh(\alpha\delta) + \cos(\alpha\delta)]\right\} + \left[\frac{T_3 - T_{-3} + T_1 - T_{-1}}{4(T_1 - T_{-1})}\right] = 0. \tag{18}$$

Combining Eqs. (14) and (18) now results in a quadrative equation with respect to the cosine function, which is written as

$$a\cos^2(\alpha\delta) + b\cos(\alpha\delta) + c = 0, \tag{19}$$

where

$$a = 4T_1^2 - 4T_{-1}^2 + 4T_{-2}T_0 - 4T_0T_2, \tag{20}$$

$$b = 2T_{-2}T_{-1} - 2T_{-2}T_1 + 2T_{-1}T_0 - 2T_0T_1 + 2T_{-1}T_2 - 2T_1T_2 + 2T_0T_3 - 2T_{-3}T_0 \tag{21}$$

and

$$c = T_{-1}^2 - T_1^2 + T_2^2 - T_{-2}^2 + T_{-3}T_{-1} - T_{-1}T_3 + T_{-3}T_1 - T_1T_3 + 2T_0T_2 - 2T_{-2}T_0. \tag{22}$$

Eq. (19) is now solved using

$$\cos(\alpha\delta) = \frac{-b \pm \sqrt{b^2 - 4ac}}{2a} = \phi, \tag{23}$$

where ϕ is typically a complex number. Based on the sign in front of the radical, Eq. (23) contains two solutions to Eq. (19). Numerical simulations without noise suggest that only one solution will have an absolute value less than unity. Numerical simulations with noise and actual data (presented later) show that the absolute value of both roots can be less than unity. The root that corresponds to the flexural wavenumber can be determined by two methods. The first method involves a simple inspection, whereby one of the solutions can be eliminated due to an unrealistic value for the wavenumber. The second method computes an estimated value of the field at a sensor location using both the positive and negative roots and then determines the residual value of both estimated models and the data. The smaller residual will correspond to the correct flexural wavenumber.

The inversion of Eq. (23) allows the complex-valued flexural wavenumber α to be solved as a function of ϕ at every frequency for which a measurement is made. The solution to the real part of α is

$$\mathrm{Re}(\alpha) = \begin{cases} \frac{1}{2\delta}\,\mathrm{Arccos}(s) + \frac{n\pi}{2\delta}, & n \text{ even}, \\ \frac{1}{2\delta}\,\mathrm{Arccos}(-s) + \frac{n\pi}{2\delta}, & n \text{ odd}, \end{cases} \tag{24}$$

where

$$s = [\mathrm{Re}(\phi)]^2 + [\mathrm{Im}(\phi)]^2 - \sqrt{\left\{[\mathrm{Re}(\phi)]^2 + [\mathrm{Im}(\phi)]^2\right\}^2 - \left\{2[\mathrm{Re}(\phi)]^2 - 2[\mathrm{Im}(\phi)]^2 - 1\right\}}, \tag{25}$$

n is a non-negative integer, and A denotes the principal value of the inverse cosine function. The value of n is determined from the function s, which is a periodically varying cosine function with respect to frequency. That is, while n is 0 at zero frequency, it increases by 1 every time s cycles through π radians (180°). It is noted here that increasing the integer n allows the estimation process to be used beyond the Nyquist spacing criteria of the sensors because n keeps a record of the number of aliasing cycles between the sensors and thus accounts for these cycles in the

measurement process. After the solution to the real part of α is found, the solution to the imaginary part of α is written as

$$\mathrm{Im}(\alpha) = \frac{1}{\delta}\log e\left\{\frac{\mathrm{Re}(\phi)}{\cos[\mathrm{Re}(\alpha)\delta]} - \frac{\mathrm{Im}(\phi)}{\sin[\mathrm{Re}(\alpha)\delta]}\right\}. \tag{26}$$

The real and imaginary parts of α from Eqs. (24) and (26), respectively, are combined to yield the complex flexural wavenumber.

Although normally considered less important than the estimate of the flexural wavenumber, the response coefficients are next determined with either an exact or ordinary least-squares solution. The exact solution is found by combining Eqs. (12) and (13), which results in

$$A = \frac{2T_0\cosh(\alpha\delta) - (T_1 + T_{-1})}{2[\cosh(\alpha\delta) - \cos(\alpha\delta)]} \tag{27}$$

and

$$C = \frac{(T_1 - T_{-1}) - 2T_0\cos(\alpha\delta)}{2[\cosh(\alpha\delta) - \cos(\alpha\delta)]}. \tag{28}$$

Combining Eqs. (15) and (16) yields

$$B = \frac{2(T_1 - T_{-1})\cosh(\alpha\delta) - (T_2 - T_{-2})}{4\sin(\alpha\delta)[\cosh(\alpha\delta) - \cos(\alpha\delta)]} \tag{29}$$

and

$$D = \frac{(T_2 - T_{-2}) - 2(T_1 - T_{-1})\cos(\alpha\delta)}{4\sinh(\alpha\delta)[\cosh(\alpha\delta) - \cos(\alpha\delta)]}. \tag{30}$$

Eqs. (27)–(30) thus represent the exact estimates of the complex response coefficients.

When the second method is used to estimate these coefficients, an ordinary least-squares fit is applied to all the data points [2,6,7]. This process begins with a formulation of the problem that uses N ($=7$) algebraic equations, where N is the number of sensors. Written in matrix form, the expressions are

$$\mathbf{Ax} = \mathbf{b}, \tag{31}$$

where

$$\mathbf{A} = \begin{bmatrix} \cos(3\alpha\delta) & -\sin(3\alpha\delta) & \cosh(3\alpha\delta) & -\sinh(3\alpha\delta) \\ \cos(3\alpha\delta) & -\sin(2\alpha\delta) & \cosh(2\alpha\delta) & -\sinh(2\alpha\delta) \\ \cos(3\alpha\delta) & -\sin(\alpha\delta) & \cosh(\alpha\delta) & -\sinh(\alpha\delta) \\ 1 & 0 & 1 & 0 \\ \cos(\alpha\delta) & \sin(\alpha\delta) & \cosh(3\alpha\delta) & \sinh(\alpha\delta) \\ \cos(2\alpha\delta) & \sin(2\alpha\delta) & \cosh(2\alpha\delta) & \sinh(2\alpha\delta) \\ \cos(3\alpha\delta) & \sin(3\alpha\delta) & \cosh(\alpha\delta) & \sinh(3\alpha\delta) \end{bmatrix}, \tag{32}$$

$$\mathbf{x} = \begin{bmatrix} A \\ B \\ C \\ D \end{bmatrix}, \quad \mathbf{b} = \begin{bmatrix} T_{-3} \\ T_{-2} \\ T_{-1} \\ T_0 \\ T_1 \\ T_2 \\ T_3 \end{bmatrix}. \tag{33-34}$$

The solution to Eq. (31) is

$$\mathbf{x} = (\mathbf{A}^{\mathrm{H}}\mathbf{A})^{-1}\mathbf{A}^{\mathrm{H}}\mathbf{b}, \tag{35}$$

where the superscript H denotes the complex conjugate transpose of the matrix. The least-squares method (Eqs. (31)–(35)) is normally considered to be more accurate than the exact-solution method shown in Eqs. (27)–(30) and is therefore used for the calculations in the remainder of the paper. This increase in accuracy occurs because all the seven data points are used to estimate the response coefficients rather than only the five data points used for the exact solution. It is noted that the above procedure for estimating flexural wavenumber and response coefficients from the data provides a series of closed-form equations.

3. Numerical simulations

The inverse method is first examined with a numerical simulation that has noise added to the transfer functions. In this configuration, the beam has both ends constrained to the ground with translational springs. The baseline problem has a rectangular cross-section with the following physical properties: $E = 10^{11}(1 + 0.05\mathrm{i})\,\mathrm{N/m^2}$, $\rho = 5000\,\mathrm{kg/m^3}$, $A_b = 0.015\,\mathrm{m^2}$, $I = 2.81 \times 10^{-5}\,\mathrm{m^4}$, $L = 4\,\mathrm{m}$, $\delta = 0.5\,\mathrm{m}$, $k_1 = 10^8\,\mathrm{N/m}$, and $k_2 = 10^{12}\,\mathrm{N/m}$. To study the effects of errors, random numbers are added to the transfer functions according to the equation

$$T_e(\omega) = T(\omega) + e\{\mathrm{Re}[T(\omega)]\sigma_a + \mathrm{i}\,\mathrm{Im}[T(\omega)]\sigma_b\}, \tag{36}$$

where e is the amount of error added to the transfer function and σ_a and σ_b are random numbers with zero mean and a variance of one. The value e is also called the noise value as it represents the amount of noise added to the transfer function (or additive noise). Fig. 1 is a plot of the estimated and actual values of flexural wavenumber α versus frequency using an error value of $e = 0.02$. The actual values (no noise) of the real part of α are shown as a solid line, and the estimated values (with noise) of the real part of α are depicted with square symbols. The actual values of the imaginary part of α are shown as a solid line, and the estimated values of the imaginary part of α are depicted with circle symbols.

The effect of estimation error versus frequency is shown in Fig. 2, which is displayed with a log scale on the y-axis. The estimation error at each frequency was defined by the equation

$$\theta(\omega_m) = \frac{|\gamma_a(\omega_m) - \gamma_e(\omega_m)|}{|\gamma_a(\omega_m)|}, \tag{37}$$

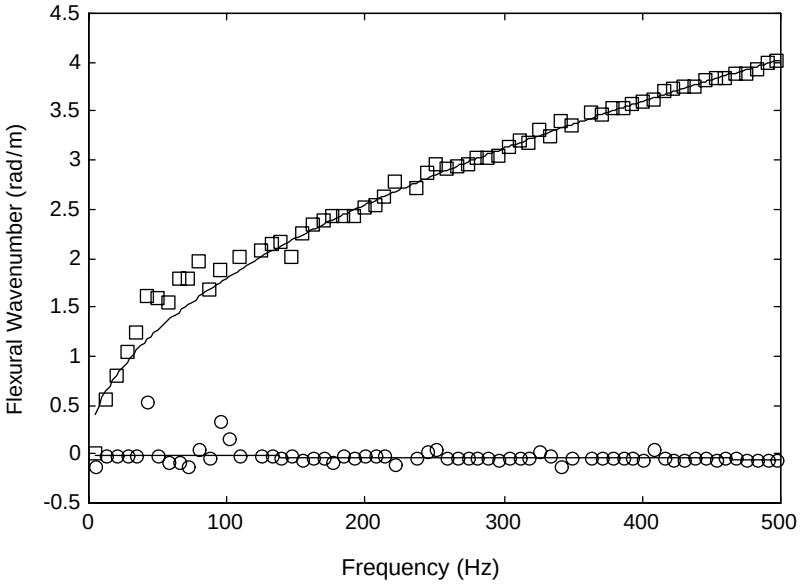

Fig. 1. Flexural wavenumber versus frequency for the numerical simulation. □, estimated real flexural wavenumber, ○, estimated imaginary flexural wavenumber, and ——, exact real and imaginary flexural wavenumbers.

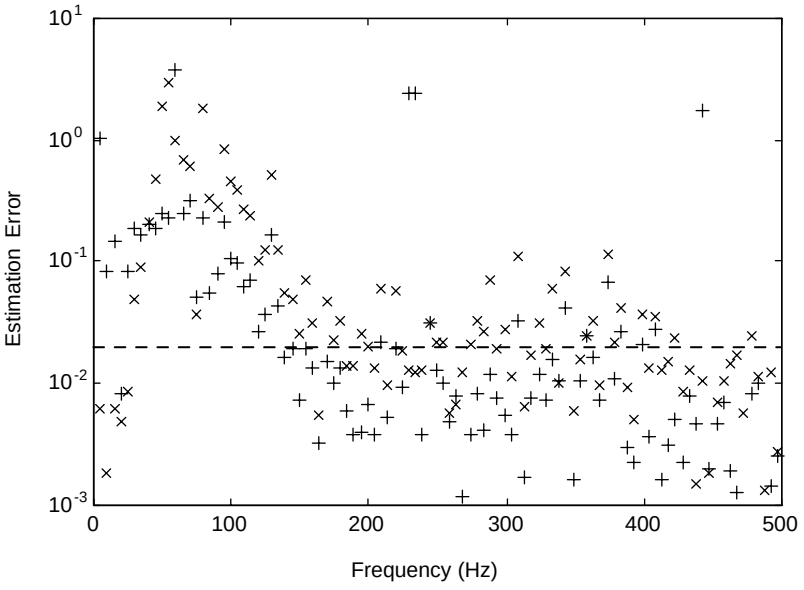

Fig. 2. Estimation error versus frequency for the numerical simulation. +, estimation error of wavenumber, ×, estimation error of displacement, and ----, the value 0.02.

where γ is either flexural wavenumber α or beam displacement U at $x = -2\delta$; $\theta(\omega_m)$ is the estimation error at the mth frequency; the subscript a corresponds to the actual (noiseless) value, and the subscript e corresponds to the estimated (calculated) value. In Fig. 2, the + symbols show flexural wavenumber estimation errors, the × symbols depict beam displacement estimation

errors, and the dashed line is the value 0.02, which is the amount of additive noise in the transfer functions. Note that the larger estimation errors tend to be seen at the lower frequency values. This condition occurs because the wavelengths are longer at lower frequencies, which produces transfer functions that have less amplitude and phase mismatch at each sensor location, thus accentuating the effects of any errors. At higher frequencies, the wavelengths become smaller, which produces transfer functions that have large amplitude and phase mismatch, thus mitigating the effects of the errors. Once the flexural wavelength is less than the aperture of the sensors (3.5 m), which occurs at approximately 100 Hz, the majority of the errors are less than 2 percent and only several are greater than 10 percent.

It is noted, from Fig. 1, that the relative errors of the imaginary part of the flexural wavenumber are much greater than the relative errors of the real part of the flexural wavenumber. This is not problematic because the wavenumber in this simulation and the following experiment are dominated by the real components and have extremely small imaginary components. Large errors in the imaginary component of extremely small imaginary flexural wavenumbers do not propagate into the transfer functions as large estimation errors.

Finally, several numerical simulations were conducted to determine the effects of sensor position error on the estimation process. A 10-percent error in the position of the middle sensor resulted in a 2-percent error in the estimation of wavenumber and a 6-percent error in the estimation of the transfer function. A $+5$-percent error in the position of two of the sensors and a -5-percent error in the position of two additional sensors (for a total of four sensors) resulted in a 14-percent error in the estimation of the wavenumber and a 12-percent error in the estimation of the transfer function. An alternating ± 1-percent error in the position of all the seven sensors resulted in an 18-percent error in the estimation of the wavenumber and a 14-percent error in the estimation of the transfer function.

4. Experiment

An experiment was conducted to test the validity of the inverse method when it was applied to actual laboratory data. A rectangular aluminum beam, mounted to a shaker table using rigid aluminum mounts at each end, had the following properties: $A_b = 0.0077\,\mathrm{m}^2$, $I = 6.66 \times 10^{-6}\,\mathrm{m}^4$, $L = 1.07\,\mathrm{m}$ and $\delta = 0.133\,\mathrm{mm}$. It is important to note that this type of mounting system does not correspond to a translational spring boundary condition but rather to a combination of translational and rotational spring boundary conditions that are acting together at each end of the beam. Because the inverse method is independent of boundary conditions, this type of unknown and mixed boundary condition does not adversely impact the measurement process.

During the measurement process, eight equally spaced accelerometers were attached to the beam. The first accelerometer served as the reference measurement to the middle seven accelerometers, which correspond to Eqs. (5)–(11). Data taken in the time domain and transferred into the frequency domain using a Fourier transform were collected by the accelerometers from 4 to 400 Hz in swept-sine mode.

Fig. 3 is a plot of the modelled and estimated values of flexural wavenumber α versus frequency. The modelled values of the real part of α are depicted with a solid line, and the estimated values are shown as square symbols. The modelled values of the imaginary part of α are depicted with a

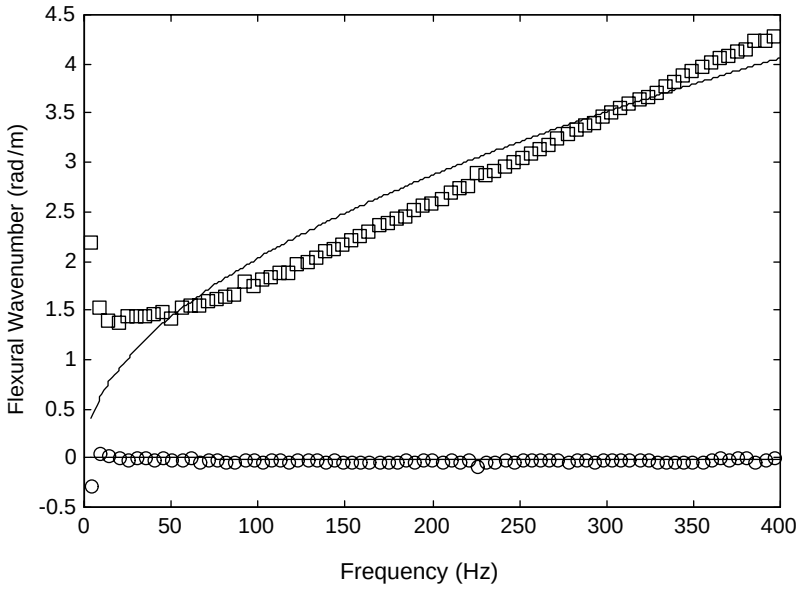

Fig. 3. Flexural wavenumber versus frequency for the experiment. □, estimated real flexural wavenumber, ○, estimated imaginary flexural wavenumber, and ——, modelled real and imaginary flexural wavenumbers.

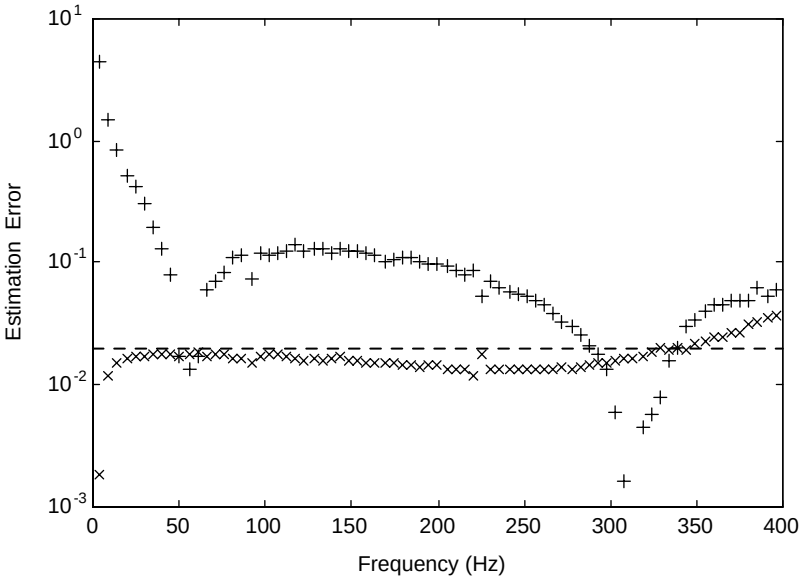

Fig. 4. +, Estimation error and normalized residual versus frequency for the experiment. +, estimation error of wavenumber, ×, normalized residual of displacement, and ----, the value 0.02.

solid line, and the estimated values are shown as circle symbols. The modelled values were determined by assuming that the aluminum bar had a Young's modulus of $7.31 \times 10^{10}(1+0.01\mathrm{i})\,\mathrm{N/m^2}$ and a density of $2700\,\mathrm{kg/m^3}$ and then calculating the (modelled) wavenumber with Eq. (4). It is noted that at low frequency there is some disagreement between the

model and the estimate, which was explained in Section 3 and also discussed by McDaniel and Shepard [9]. The estimation error versus frequency is shown in Fig. 4. In this figure, the + symbols show flexural wavenumber estimation errors based on assumed values of aluminum, the × symbols are normalized beam displacement residuals based on a model calculated using the estimated parameters and the actual data at $x = -2\delta$, and the dashed line is the value 0.02 which is included to allow cross-reference to Fig. 2.

5. Conclusions

This paper describes the derivation of an inverse method to measure the complex flexural wavenumber and response coefficients of a beam. The new approach obtains seven measured transfer functions by vibrating the beam transversely with any set of corresponding boundary conditions. These measurements are then combined to yield closed-form solutions of the beam parameters. Numerical simulations were presented to show the results of the method with noise in the simulated data, and an experiment has validated the effectiveness of the technique when it is applied to laboratory data.

Acknowledgements

This work was funded by the Office of Naval Research. The authors wish to thank Gerald Messina for his assistance in setting up the experiment and collecting the data and Karen Holt for her help with the technical editing. Additionally, they wish to thank the reviewers whose comments measurably improved the paper.

References

[1] G.R. de Prony, Essai éxperimental et analytique: sur les lois de la dilatabilité de fluides élastique et sur celles de la force expansive de la vapeur de l'alkool à différentes températures, Journal de l'École Polytechnique 1 (22) (1795) 24–76.
[2] K. Grosh, E.G. Williams, Complex wave-number decomposition of structural vibrations, Journal of the Acoustical Society of America 93 (2) (1993) 836–848.
[3] Y.M. Ram, Inverse mode problems for the discrete model of a vibrating beam, Journal of Sound and Vibration 169 (2) (1994) 238–252.
[4] J. Linjama, T. Lahti, Measurement of bending wave reflection and impedance in a beam by the structural intensity technique, Journal of Sound and Vibration 161 (2) (1993) 317–331.
[5] P.D. Bauman, Measurement of structural intensity: analytic and experimental evaluation of various techniques for the case of flexural waves in one-dimensional structures, Journal of Sound and Vibration 174 (5) (1994) 677–694.
[6] B.R. Mace, C.R. Halkyard, Time domain estimation of response and intensity in beams using wave decomposition and reconstruction, Journal of Sound and Vibration 230 (3) (2000) 561–589.
[7] L.L. Koss, D. Karczub, Beam bending wave solution predictions of dynamic strain using frequency response functions, Journal of Sound and Vibration 184 (2) (1995) 229–244.
[8] J.G. McDaniel, P. Dupont, L. Salvino, A wave approach to estimating frequency-dependent damping under transient loading, Journal of Sound and Vibration 231 (2) (2000) 433–449.
[9] J.G. McDaniel, W.S. Shepard Jr., Estimation of structural wave numbers from spatially sparse response measurements, Journal of the Acoustical Society of America 108 (4) (2000) 1674–1682.